

Article pubs.acs.org/acsaelm

Strong Electronic Coupling of Graphene Nanoribbons onto Basal Plane of a Glassy Carbon Electrode

Marija R. Zoric, Erik J. Askins, Xiaoxiao Qiao, and Ksenija D. Glusac*



Cite This: ACS Appl. Electron. Mater. 2021, 3, 854–860



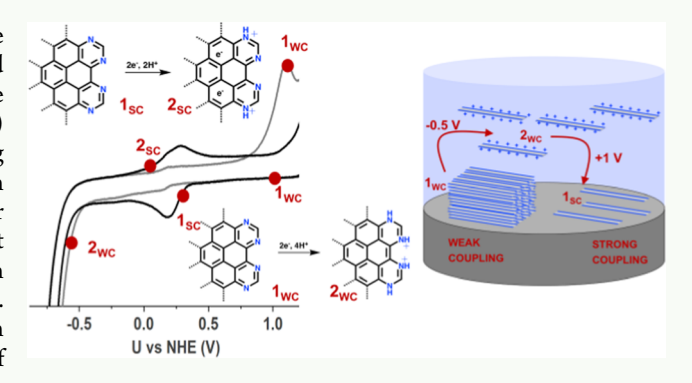
ACCESS I

III Metrics & More

Article Recommendations

Supporting Information

ABSTRACT: The grafting of molecular motifs to the conductive carbon represents a promising approach toward improved hybrid materials for electrocatalytic applications. Here, we investigate the electrochemical behavior of graphene nanoribbons (GNR) deposited onto a glassy carbon electrode using π - π stacking interactions. Using the bipyrimidine moiety on the nanoribbon edges as a reporter of the proton-coupled electron transfer chemistry, we illustrate that the simple electrochemical treatment of as-deposited nanoribbon generates a hybrid material that is in strong electronic communication with the conductive support. This work shows a strategy for modifying the basal plane of carbon materials and provides a potential platform for the incorporation of catalytic metal sites via coordination through the N-functionalities of GNR.



KEYWORDS: graphene nanoribbons, carbon electrode modification, strong electronic coupling, electrochemical treatment, proton-coupled electron transfer

■ INTRODUCTION

Graphitic nanocarbon materials have recently been recognized as promising electrocatalysts for a range of useful transformations, such as the reduction of dioxygen to water, dinitrogen to ammonia, and carbon dioxide to methanol. 1-3 The success of these electrode materials is attributed to the high electronic conductivity of graphitic carbon, the high surface area of nanocarbon electrodes made using templatedirected pyrolysis, and the presence of reactive catalytic functional groups obtained by heteroatom doping of otherwise chemically inert carbon framework. Further progress in the field requires the synthesis of nanocarbon electrodes with complex multinuclear catalytic motifs that go beyond "singleatom catalysts." Unfortunately, the introduction of such welldefined catalytic functionalities is limited by the extreme temperatures required to graphitize carbon precursors, at which most functional groups undergo decomposition.

A more favorable way to introduce catalytic moieties to graphitic electrodes involves postpyrolysis modifications of carbon edge and basal sites with well-defined molecular motifs. For this purpose, several creative chemical methods have been developed to immobilize molecular catalysts to the carbonbased surfaces using covalent bonds, $^{4-11}$ $\pi-\pi$ stacking, $^{12-19}$ and electrostatic interactions.^{20,21} Carbon edge sites are often modified covalently using "click" chemistry 4,7 or aryl radical intermediates formed from diazonium salts. 5,6 Carbon basal sites are modified using π - π stacking interactions between polyaromatic groups, most commonly pyrene, and the carbon electrode. Here, the catalytic units are connected to pyrene through an alkyl chain. 15-17,19 These modification techniques ensure the immobilization of homogeneous catalysts, thus eliminating the need for their diffusion to the electrode surface. However, the electrochemical behavior of such immobilized catalysts usually does not differ from that observed in homogeneous analogs because the electronic coupling between the catalytic moieties and the conductive carbon electrode remains weak.

More recently, chemical methods have been explored to graft molecular catalysts using strong electronic coupling to create new hybrid structures with altered reactivity and catalytic behavior. Specifically, Compton and co-workers showed that the carbon edge planes can be functionalized using ortho-quinone groups generated by the anodic treatment of the electrode surface.²² The Surendranath group used this coupling method to attach molecular catalysts to the carbon edge sites and found that the strong electronic coupling exists between the catalytic unit and the carbon band structures. ^{23–25}

Received: November 6, 2020 Accepted: January 8, 2021 Published: January 20, 2021





Such strong coupling resulted in interesting changes of the electrochemical behavior of the grafted hybrid relative to the homogeneous analog. For example, grafted hybrids were shown not to undergo simple outer-sphere electron transfer processes, which in turn had important implications in catalysis by enabling the proton-coupled chemistry to take place: a hydrogen-evolving Rh-based catalyst, when grafted to the carbon electrode, operates over a full pH region (0-14), whereas the homogeneous analog shows catalytic activity only in the acidic region. $^{23-25}$

Similar mechanistic studies involving basal plane modifications and the strong electronic coupling regime are scarcer. Several recent reports involving immobilized metal-coordinated N_4 -macrocycles indicate that the π -stacking interactions may generate strongly coupled hybrids. 26-34 For example, the coupling of molecular cobalt phthalocyanine, a carbon dioxide reduction catalyst, to a carbon nanotube support has been shown to affect product selectivity: two-electron reduction to CO is favored when the homogeneous catalyst is used, while a six-electron reduction to methanol takes place with the heterogeneous catalyst/carbon hybrid.²⁶ Similar studies with immobilized metal-coordinated N₄ macrocycles have shown better efficiency toward CO₂ reduction to CO₂²⁷⁻³² as well as improved nitrogen reduction reaction efficiency.³³ However, most of those basal plane modification studies have been focused on catalytic performance rather than a mechanistic investigation of their fundamental electrochemistry.

Here, we investigate the degree of electronic coupling in molecule/carbon electrode hybrids functionalized using π -stacking interactions. Specifically, we explore how the electrochemical behavior of 4,4'-bipyrimidine (BPM) changes when immobilized to the glassy carbon surface using graphene nanoribbon linkers (GNR, Scheme 1). GNRs exhibit large planar aromatic structures capable of π - π stacking with the

Scheme 1. Structures of Model Compounds (BPM and GNR) and the Products of Their Cathodic Reduction via Two-Electron, Two-Proton (BPMH₂ and GNRH₂) and Two-Electron Four-Proton (BPMH₄²⁺ and GNRH₄²⁺) Transfer Chemistry

GNR

basal sites of the carbon electrode, while the redox activity of bipyrimidine functionalities reports on the degree of electronic coupling between the nitrogen sites and the electrode surface. Our detailed studies of proton-coupled electron transfer (PCET) chemistry of nitrogen moieties reveal that the electrochemically treated GNRs form monolayers that are strongly coupled with the carbon electrode. This work shows a novel strategy for modifying the basal plane of carbon materials and provides a potential platform for the incorporation of catalytic metal sites via coordination through the N-functionalities of GNR.

■ RESULTS AND DISCUSSION

GNR was synthesized according to the method published by Sinitskii and co-workers (SI, Scheme S1).35 The procedure involves the synthesis of a soluble aryl-substituted benzene monomer 8 via Diels-Alder cycloaddition/decarbonylation sequence developed by Müllen and co-workers.³⁶ Dibrominated monomer 8 was then subjected to Yamamoto coupling to produce soluble polymer 9. The matrix-assisted laser desorption/ionization (MALDI) mass spectrum of polymer 9 reveals a series of oligomer peaks, separated by 522 au (corresponding to the mass of one monomer unit), with sizes up to 16 monomer units corresponding to ~20 nm length (Figure S1, SI). The sample of polymer 9 may contain longer chains that are not detectable by mass spectrometry, and this hypothesis is consistent with the previous reports of micrometer-long nanoribbons obtained using similar Yamamoto coupling procedures. 35,37 The oxidative cyclodehydrogenation of polymer 9 yielded insoluble GNR, which was characterized using solid-state NMR, Raman spectroscopy, transmission electron microscopy, and X-ray photoelectron spectroscopy (XPS) (Figures S2–S5, SI).

Electrochemical behavior of BPM was studied using cyclic voltammetry (CV) in an aqueous medium (black traces in Figures 1 and S6). Chemically reversible or quasi-reversible reduction features were observed in the cathodic region (-0.5)to 0 V vs NHE), and the half-wave potential was found to shift to more negative values with increasing pH, indicative of PCET. The equilibrium potentials were used to construct the Pourbaix diagram in Figure 2A, which shows two distinct pH regions (0-4 and 4-14) in which the potential varies linearly with pH. The experimental data were fit to the Nernst equation for PCET, 38 which lead to the assignment of the two pH regions as follows: the pH = 4-14 process was assigned to a two-electron two-proton transfer reduction to form BPMH₂, while the acidic pH = 0-4 region was assigned to the twoelectron four-proton-coupled reduction to form BPMH₄²⁺ (Scheme 1). This conclusion was further supported by an excellent match between the standard reduction potential $E_{\rm PCET}^0$ obtained from the Pourbaix diagram and the same parameter calculated using standard reduction potentials for single-electron transfer processes and the relevant pK_a values (more information is available in Tables S1 and S2 of Section S4B, Supporting Information, SI).

The electrochemical behavior of as-deposited GNR is significantly different from BPM (red traces in Figures 1, S7, and S8). For example, the CV of GNR collected at pH = 1 exhibits an intense cathodic peak at $E_{\rm c} = -0.752$ V and a weaker anodic peak at $E_{\rm a} = 1.074$ V. This large separation between the cathodic and anodic peaks indicates a large kinetic barrier for the observed electrochemical transformation. Interestingly the approximate half-wave potential for GNR is

GNRH₄24

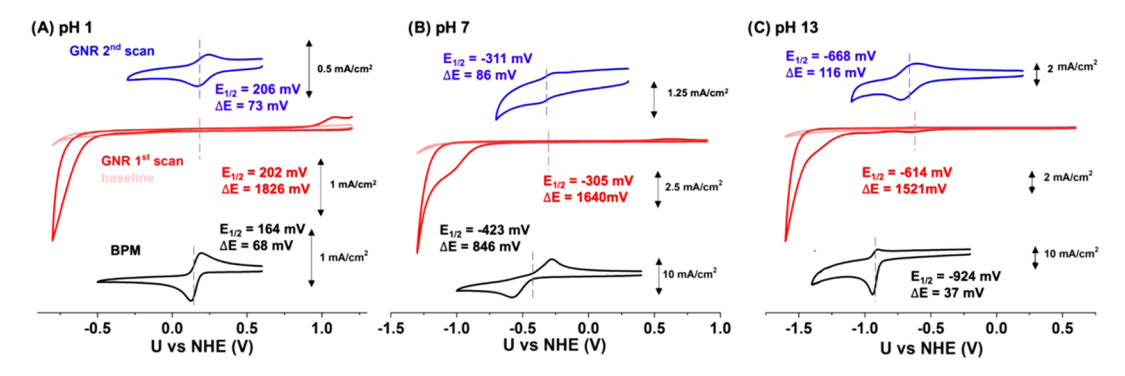


Figure 1. CVs of BPM (black), as-deposited GNR (red), and second-scan GNR (blue) in 1 M aqueous solutions at pH 1 (A), pH 7 (B), and pH 13 (C). GC working electrode; 100 mV/s scan rate. Background scans are shown in pale red in all three panels.

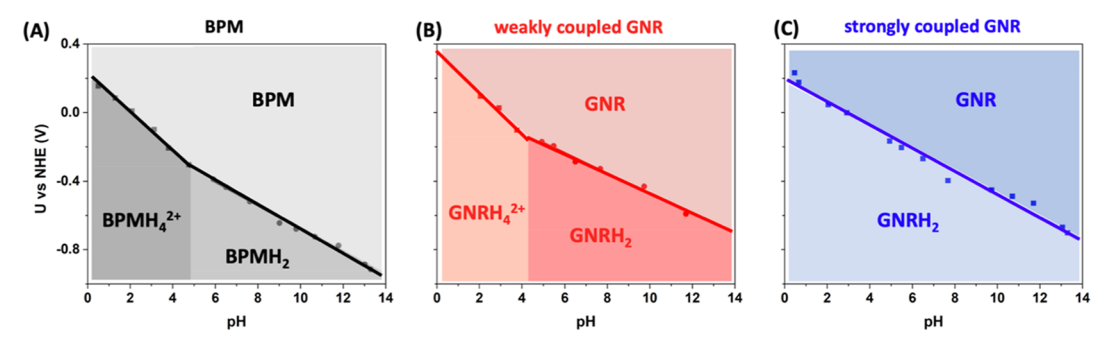


Figure 2. Pourbaix diagrams of (A) BPM, (B) GNR weakly coupled to the electrode, and (C) GNR strongly coupled to the electrode. Shaded parts represent pH-potential regions where annotated species are stable.

similar ($E_{1/2} = 202 \text{ mV}$) to that observed in BPM ($E_{1/2} = 164 \text{ mV}$). Furthermore, the half-wave potential shifts to more negative potentials with increasing pH, suggesting that the observed transformation is the proton-coupled reduction of bipyrimidine moieties in GNR. The slow rate for the observed PCET is likely associated with the low electron and proton conductivity in GNR aggregates in the as-deposited sample. Similar sluggish kinetics were observed in studies of phthalocyanine aggregates, ^{29,39} and these results illustrate the need for the development of deposition methods that ensure monomolecular coverage of molecular units and good electronic communication with the carbon support.

Interestingly, the cathodic (I_c) and anodic (I_a) peak currents in as-deposited GNR are not the same. For example, I_c/I_a in the CV of GNR at pH = 1 is 7, indicating that some of the GNR material is detached from the electrode surface upon reduction. This prompted us to investigate the electrochemical behavior of GNR upon subsequent scans (blue traces in Figures 1 and S7–S9). The CVs of GNR after the first CV scan are significantly different from those for as-deposited GNR. Namely, the second-scan CVs show the appearance of new reversible and pH-dependent features in the 0 to -1 V potential range. These reversible features in the second scan appear only if the first scan ends at potentials more positive than the anodic process (Figure S10), suggesting that their formation requires reduction and reoxidation of as-deposited GNR, and are assigned to the monolayer GNR deposited to the carbon support by electrochemical cycling. This assignment is based on the fact that the anodic-cathodic peak potential separation ΔE is drastically reduced in the secondscan features, suggesting that the kinetics of electron and proton transfer are significantly improved. Furthermore, the integration of CV peaks is consistent with the expected current

for the 0.5–3 monolayer GNR coverage (Section S4). Based on these experimental findings, we hypothesize that the electrochemical reduction of as-deposited GNRs causes their partial desorption and solubilization in the solution above the electrode surface. The subsequent reoxidation of solubilized GNRH₄²⁺ results in their redeposition to the electrode surface, causing improved electronic coupling to the carbon electrode support (as illustrated in Figure 4). This simple electrochemical treatment provides a promising method toward the deposition of molecular species to the carbon electrode and can be useful to the field of molecular enhancement of heterogeneous electrocatalysis.⁴⁰ Interestingly, the analogous anodic pretreatment does not produce strongly coupled GNRs (Figure S13, SI).

Due to its large aromatic and planar structure, GNR is likely held to the GC electrode via π - π interactions. This conclusion is further supported by the results of a comparative study involving GC electrodes with covalently attached imine groups. Pyrazine-modified electrodes were prepared as previously described, 46 and CVs were run on this electrode as prepared and after sonication (Figure S12B, SI). It is shown that this modification is stable even after 30 min of sonication. On the other hand, GNR-modified GC does not show the strongly coupled GNR peak after only 10 min of sonication (Figure S12A). These experiments do not directly show that GNR has π - π interactions with GC, but it proves they are weaker than covalent modifications. Interestingly, GNRs interact with both the basal and the edge plane of the carbon electrode. In specific, highly ordered pyrolytic graphite (HOPG) electrodes were also modified with GNR to probe the type of interactions between the electrode and GNRs. The same electrochemical treatment was performed on HOPG basal and edge plane electrodes as was done on GC, but no significant difference between GC and basal and edge plane HOPG was noticed (Figure S15, SI).

We now seek to answer the following question: does deposited GNR behave like the molecular species in solution or does it undergo the field-induced electrochemistry observed previously²³⁻²⁵ for molecular species that are in strong electronic communication with the electrode? To address this, we compared Pourbaix diagrams for as-deposited GNRs (first CV scan) and monolayer GNRs (second CV scan). The Pourbaix diagram of as-deposited GNRs (Figure 2B) show that their half-wave potentials are slightly more positive than the corresponding potentials for BPM, and this shift is assigned to the extended conjugation of GNR. Aside from this difference, the Pourbaix diagrams of BPM and as-deposited GNR exhibit similar pH-dependence, indicative of GNRH2 formation in the pH = 4-14 range and GNRH₄²⁺ formation in the 0-4 region (Scheme 1). The two-electron, four-proton reduction behavior observed in the pH = 0-4 region is indicative of weak electronic coupling between GNR and the carbon support. When the strong electronic coupling is achieved, each proton transfer event generates a surface charge that is immediately compensated by the electron transfer from the electrode, leading to an overall neutral product and the 59 mV/pH slope in the Pourbaix diagram.²⁵ Again, the additional support of the PCET assignment in weakly coupled GNR was provided by obtaining a good match between the experimental E_{PCET}^0 values and those calculated using DFT (Tables S3 and S4 in Section S4B).

The Pourbaix diagram of the second CV-scan GNR (Figure 2C) is different from that obtained for as-deposited GNRs. In specific, the slope of the Pourbaix diagram remains the same throughout the entire pH = 0-14 range. The change in PCET chemistry that was observed at ~pH 4 in the case of BPM and as-deposited GNR was absent. We hypothesize that this behavior indicates that the second CV-scan GNR is strongly coupled with the carbon support. As mentioned earlier, the strongly coupled system is expected to only undergo processes that are overall charge neutral-each protonation of the surface nitrogen sites triggers the immediate charge compensation by electrons from the carbon electrode. 23-25 Thus, the absence of the two-electron, four-proton-coupled chemistry in the acidic region is indicative of the strong coupling regime. The exact number of protons (m) and electrons (n) transferred during PCET is difficult to evaluate from Figure 2C because the \sim 59 mV/pH slope informs only of the m/n = 1 ratio. To obtain more insight into the details of the process, the Pourbaix diagram was treated using the model developed by Surendranath for field-driven PCET. 24,25 Based on this model, the E_{PCET}^0 can be estimated from the potential of zero free charge for the electrode/electrolyte interface and the zero-field pK, values of the surface protonation sites. We applied this model to two possible PCET scenarios, one where two protons and electrons are transferred and another where four protons and electrons are transferred (Section S4B, SI). A better match with the experiment was observed for two-proton/electron PCET, indicating the likelihood that only two nitrogen centers are protonated.

XPS investigations on modified carbon electrodes were conducted to provide additional insight into the electrochemical behavior of GNRs (experimental details are presented in Section S5). Electrodes were prepared by depositing GNR in different thickness regimes, to investigate both the weakly coupled GNR aggregates and strongly coupled

GNR monolayers. The sample thickness had a profound effect on the observed N 1s peaks (Figure 3A). Specifically, the thick

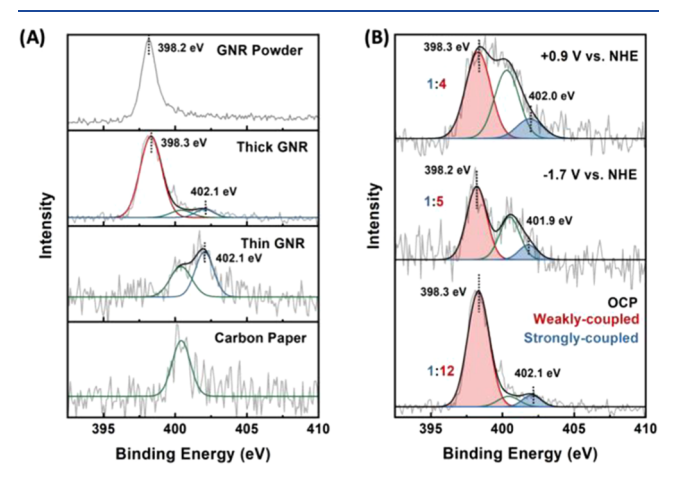


Figure 3. (A) XPS data recorded at open-circuit potential (OCP) across multiple thickness regimes. Red, blue, and green traces are used to identify the fitting of N 1s from the weakly coupled GNR, strongly coupled GNR, and carbon electrode, respectively. (B) Ex situ XPS data at OCP, cathodic and anodic potentials for thick GNR electrodes with ratios of strongly and weakly coupled GNR signals.

sample showed a major peak at 398.3 eV (red), which we attribute to pyridinic N atoms. 35,41 The same peak was observed for GNR powder, indicating that it originates from GNR aggregates that are not coupled to the carbon electrode. The thick sample had additional higher binding energy (BE) features at 402.1 (blue) and 400.4 eV (green). The 400.4 eV feature was observed on the bare electrode, and it arises due to native nitrogen present in commercial carbon electrodes.⁴ The 402.1 eV peak is assigned to the signal from monolayer GNR. This assignment is consistent with the appearance of the N 1s peak at higher BE, a trend that is expected for GNR in intimate electronic interaction with the electron-withdrawing electrode environment. 43,44 Meanwhile, the thin sample only shows features from the strongly coupled monolayer GNR and the nitrogen present on the bare electrode (Figure 3A), further confirming our assignment of 398.3 and 402.1 eV peaks to those arising from aggregate and monolayer GNRs, respectively.

The changes in the XPS N 1s peaks of thick GNR samples were monitored after electrochemical treatment (Figure 3B). The samples, initially at open-circuit potential (OCP), were first reduced at a constant potential of -1.7 V, then reoxidized at a constant potential of +0.9 V. The N 1s XPS data were collected at three potentials to observe changes to the sample. Interestingly, cathodic treatment, which gives rise to PCET, does not lead to any significant shift in BE from the weakly or strongly coupled signals. The lack of the shift in the red signal after the -1.7 V treatment is not surprising, as it is assigned to the residual GNR aggregates on the electrode which were not electrochemically reduced. We hypothesize that the reduced GNR detaches from the electrode and thus not contribute to the XPS signal. The lack of the shift in the blue signal is more surprising, as it originates from strongly coupled GNRs which have participated in PCET. The observed insensitivity of the N 1s BE indicates that the effect of nitrogen protonation on BE is fully compensated by the electron density redistribution within the carbon electrode, resulting in a near-zero BE shift (Figure 4). This finding is similar to in situ studies on strongly coupled

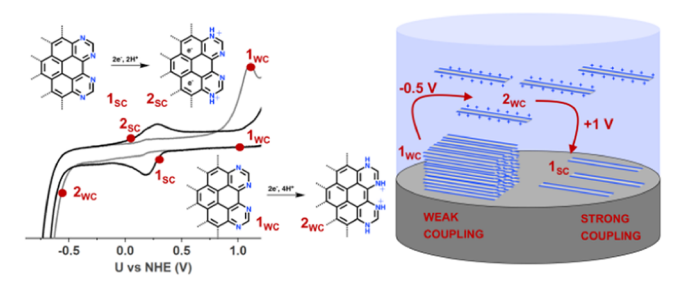


Figure 4. Electrochemical behavior of GNR on the GC electrode. The gray line presents the first CV scan, while the black line is the second scan at pH 1. The red dots present certain points where the transformation of interest occurs with insets showing corresponding relevant structural motifs. $_{\rm WC}$ and $_{\rm SC}$ stand for weakly and strongly coupled GNR, respectively.

Rh-functionalized GC electrodes where, unlike their molecular analogs, no change in X-ray absorption near edge structure, i.e., oxidation state, during ion-coupled ET is observed. Similarly, subsequent anodic treatment does not induce changes to the binding energies of weakly or strongly coupled GNR. Importantly, integrated areas under XPS curves suggest that the electrochemical treatment is enriching the ratio of strongly to weakly coupled GNRs as it changes from 1:12, 1:5, and 1:4 across the OCP, cathodic, and anodic panels, respectively. These results provide additional evidence that the electrochemical treatment of GNRs leads to the improved electronic contact between GNR and the carbon support.

Based on combined electrochemical and XPS investigations, we hypothesize that strong coupling between GNR and the carbon support can be achieved via electrochemical cycling of drop-casted GNRs, as schematized for the acidic electrolyte solution in Figure 4. Upon reduction (gray line, point $2_{\rm WC}$, Figure 4), GNR is reduced to GNRH₄²⁺, which detaches from the electrode and partially dissolves in the electrolyte solution. Subsequent oxidation to GNRH₄²⁺ (point $1_{\rm WC}$) redeposits some of the GNRs onto the electrode, now in improved electronic communication with GC, showing the PCET behavior of a strongly coupled system (points $1_{\rm SC}$ and $2_{\rm SC}$).

CONCLUSIONS

In summary, we provide a mechanistic investigation of PCET in GNR/carbon electrode hybrids. Our work demonstrated that strong electronic coupling can be achieved between the molecular unit and the carbon support using noncovalent $\pi-\pi$ stacking interactions via a simple electrochemical treatment that involves cathodic/anodic cycling of as-deposited GNR. The presence of nitrogen-containing functionalities on GNR opens up the possibility to coordinate transition metals and develop a new type of heterogeneous electrocatalysts with molecular-level control of the catalytic units.

■ ASSOCIATED CONTENT

Supporting Information

The Supporting Information is available free of charge at https://pubs.acs.org/doi/10.1021/acsaelm.0c00978.

Synthetic procedure, characterization of GNR, CVs, Pourbaix diagrams (experimental and calculated data), XPS (experimental and fitting details), reduction potential and pK_a calculations, and coordinates of optimized structures (PDF)

AUTHOR INFORMATION

Corresponding Author

Ksenija D. Glusac — Department of Chemistry, University of Illinois at Chicago, Chicago, Illinois 60607, United States; Chemical Sciences and Engineering Division, Argonne National Laboratory, Lemont, Illinois 60439, United States; orcid.org/0000-0002-2734-057X; Email: glusac@uic.edu

Authors

Marija R. Zoric — Department of Chemistry, University of Illinois at Chicago, Chicago, Illinois 60607, United States; Chemical Sciences and Engineering Division, Argonne National Laboratory, Lemont, Illinois 60439, United States

Erik J. Askins — Department of Chemistry, University of Illinois at Chicago, Chicago, Illinois 60607, United States; Chemical Sciences and Engineering Division, Argonne National Laboratory, Lemont, Illinois 60439, United States

Xiaoxiao Qiao — Department of Chemistry, University of Illinois at Chicago, Chicago, Illinois 60607, United States; Chemical Sciences and Engineering Division, Argonne National Laboratory, Lemont, Illinois 60439, United States

Complete contact information is available at: https://pubs.acs.org/10.1021/acsaelm.0c00978

Notes

The authors declare no competing financial interest.

ACKNOWLEDGMENTS

This work was supported by the National Science Foundation grants 1954298 and 156597. We gratefully acknowledge the computing resources provided on Bebop, a high-performance computing cluster operated by the Laboratory Computing Resource Center at ANL.

REFERENCES

- (1) Cao, L.; Luo, Q.; Chen, J.; Wang, L.; Lin, Y.; Wang, H.; Liu, X.; Shen, X.; Zhang, W.; Liu, W.; et al. Dynamic oxygen adsorption on single-atomic Ruthenium catalyst with high performance for acidic oxygen evolution reaction. *Nat. Commun.* **2019**, *10*, No. 4849.
- (2) Xiao, M.; Zhu, J.; Li, G.; Li, N.; Li, S.; Cano, Z. P.; Ma, L.; Cui, P.; Xu, P.; Jiang, G.; et al. A single-atom iridium heterogeneous catalyst in oxygen reduction reaction. *Angew. Chem., Int. Ed.* **2019**, 131, 9742–9747.
- (3) Askins, E. J.; Zoric, M. R.; Li, K.; Luo, L.; Amine, K.; Glusac, K. D. Toward a mechanistic understanding of electrocatalytic nanocarbon., 2020.
- (4) McCrory, C. C.; Devadoss, A.; Ottenwaelder, X.; Lowe, R. D.; Stack, T. D. P.; Chidsey, C. E. Electrocatalytic O_2 reduction by covalently immobilized mononuclear copper (I) complexes: evidence for a binuclear Cu_2O_2 intermediate. J Am. Chem. Soc. **2011**, 133, 3696–3699.
- (5) Delamar, M.; Hitmi, R.; Pinson, J.; Saveant, J. M. Covalent modification of carbon surfaces by grafting of functionalized aryl radicals produced from electrochemical reduction of diazonium salts. *J. Am. Chem. Soc.* **1992**, *114*, 5883–5884.
- (6) Willkomm, J.; Bertin, E.; Atwa, M.; Lin, J.-B.; Birss, V.; Piers, W. E. Grafting of a molecular rhenium CO₂ reduction catalyst onto colloid-imprinted carbon. *ACS Appl. Energy Mater.* **2019**, *2*, 2414–2418.
- (7) Li, H.; Cheng, F.; Duft, A. M.; Adronov, A. Functionalization of single-walled carbon nanotubes with well-defined polystyrene by "click" coupling. *J. Am. Chem. Soc.* **2005**, *127*, 14518–14524.

- (8) Zhanaidarova, A.; Moore, C. E.; Gembicky, M.; Kubiak, C. P. Covalent attachment of [Ni (alkynyl-cyclam)]²⁺ catalysts to glassy carbon electrodes. *Chem. Commun.* **2018**, *54*, 4116–4119.
- (9) Zhanaidarova, A.; Ostericher, A. L.; Miller, C. J.; Jones, S. C.; Kubiak, C. P. Selective reduction of CO₂ to CO by a molecular re (ethynyl-bpy)(CO)₃Cl catalyst and attachment to carbon electrode surfaces. *Organometallics* **2019**, *38*, 1204–1207.
- (10) Jouikov, V.; Simonet, J. Novel method for grafting alkyl chains onto glassy carbon. Application to the easy immobilization of ferrocene used as redox probe. *Langmuir* **2012**, *28*, 931–938.
- (11) Kallick, J. D.; Feng, W.-J.; McCrory, C. C. Controlled Formation of Multilayer Films of Discrete Molecular Catalysts for the Oxygen Reduction Reaction using a Layer-by-Layer Growth Mechanism Based on Sequential Click Chemistry. ACS Appl. Energy Mater. 2020, 3, 6222–6231.
- (12) Maurin, A.; Robert, M. Noncovalent immobilization of a molecular iron-based electrocatalyst on carbon electrodes for selective, efficient CO_2 -to-CO conversion in water. *J. Am. Chem. Soc.* **2016**, 138, 2492–2495.
- (13) Li, F.; Zhang, B.; Li, X.; Jiang, Y.; Chen, L.; Li, Y.; Sun, L. Highly efficient oxidation of water by a molecular catalyst immobilized on carbon nanotubes. *Angew. Chem., Int. Ed.* **2011**, *50*, 12276–12279.
- (14) Blakemore, J. D.; Gupta, A.; Warren, J. J.; Brunschwig, B. S.; Gray, H. B. Noncovalent immobilization of electrocatalysts on carbon electrodes for fuel production. *J. Am. Chem. Soc.* **2013**, *135*, 18288–18291
- (15) Das, A.; Stahl, S. S. Noncovalent immobilization of molecular electrocatalysts for chemical synthesis: efficient electrochemical alcohol oxidation with a pyrene—TEMPO conjugate. *Angew. Chem., Int. Ed.* **2017**, *56*, 8892–8897.
- (16) Reuillard, B.; Ly, K. H.; Rosser, T. E.; Kuehnel, M. F.; Zebger, I.; Reisner, E. Tuning product selectivity for aqueous CO2 reduction with a Mn (bipyridine)-pyrene catalyst immobilized on a carbon nanotube electrode. *J. Am. Chem. Soc.* **2017**, *139*, 14425–14435.
- (17) Jaegfeldt, H.; Kuwana, T.; Johansson, G. Electrochemical stability of catechols with a pyrene side chain strongly adsorbed on graphite electrodes for catalytic oxidation of dihydronicotinamide adenine dinucleotide. *J. Am. Chem. Soc.* **1983**, *105*, 1805–1814.
- (18) Creus, J.; Matheu, R.; Peñafiel, I.; Moonshiram, D.; Blondeau, P.; Benet-Buchholz, J.; García-Antón, J.; Sala, X.; Godard, C.; Llobet, A. A million turnover molecular anode for catalytic water oxidation. *Angew. Chem.* **2016**, *128*, 15608–15612.
- (19) Rajabi, S.; Ebrahimi, F.; Lole, G.; Odrobina, J.; Dechert, S.; Jooss, C.; Meyer, F. Water oxidizing diruthenium electrocatalysts immobilized on carbon nanotubes—effects of the number and positioning of pyrene anchors. ACS Catal. 2020, 10, 10614–10626.
- (20) Toma, F. M.; Sartorel, A.; Iurlo, M.; Carraro, M.; Parisse, P.; Maccato, C.; Rapino, S.; Gonzalez, B. R.; Amenitsch, H.; Da Ros, T.; et al. Efficient water oxidation at carbon nanotube—polyoxometalate electrocatalytic interfaces. *Nat. Chem.* **2010**, *2*, 826–831.
- (21) Liu, Y.; McCrory, C. C. Modulating the mechanism of electrocatalytic CO₂ reduction by cobalt phthalocyanine through polymer coordination and encapsulation. *Nat. Commun.* **2019**, *10*, No. 1683
- (22) Thorogood, C. A.; Wildgoose, G. G.; Crossley, A.; Jacobs, R. M.; Jones, J. H.; Compton, R. G. Differentiating between ortho-and para-quinone surface groups on graphite, glassy carbon, and carbon nanotubes using organic and inorganic voltammetric and X-ray photoelectron spectroscopy labels. *Chem. Mater.* **2007**, *19*, 4964–4074
- (23) Jackson, M. N.; Kaminsky, C. J.; Oh, S.; Melville, J. F.; Surendranath, Y. Graphite conjugation eliminates redox intermediates in molecular electrocatalysis. *J. Am. Chem. Soc.* **2019**, *141*, 14160–14167.
- (24) Jackson, M. N.; Surendranath, Y. Molecular control of heterogeneous electrocatalysis through graphite conjugation. *Acc. Chem. Res.* **2019**, *52*, 3432–3441.

- (25) Jackson, M. N.; Pegis, M. L.; Surendranath, Y. Graphite-conjugated acids reveal a molecular framework for proton-coupled electron transfer at electrode surfaces. *ACS Cent. Sci.* **2019**, *5*, 831–841
- (26) Wu, Y.; Jiang, Z.; Lu, X.; Liang, Y.; Wang, H. Domino electroreduction of CO_2 to methanol on a molecular catalyst. *Nature* **2019**, 575, 639–642.
- (27) Wang, X.; Sun, L.; Huang, Z.; Reddu, V.; Su, T.; Fisher, A. C. A planar, conjugated N4-macrocyclic cobalt complex for heterogeneous electrocatalytic CO₂ reduction with high activity. *Angew. Chem., Int. Ed.* **2020**, *59*, 17104–17109.
- (28) Zhang, X.; Wang, Y.; Gu, M.; Wang, M.; Zhang, Z.; Pan, W.; Jiang, Z.; Zheng, H.; Lucero, M.; Wang, H.; et al. Molecular engineering of dispersed nickel phthalocyanines on carbon nanotubes for selective CO₂ reduction. *Nat. Energy* **2020**, *5*, 684–692.
- (29) Zhu, M.; Ye, R.; Jin, K.; Lazouski, N.; Manthiram, K. Elucidating the reactivity and mechanism of CO₂ electroreduction at highly dispersed cobalt phthalocyanine. *ACS Energy Lett.* **2018**, 3, 1381–1386.
- (30) Zhang, X.; Wu, Z.; Zhang, X.; Li, L.; Li, Y.; Xu, H.; Li, X.; Yu, X.; Zhang, Z.; Liang, Y.; et al. Highly selective and active CO_2 reduction electrocatalysts based on cobalt phthalocyanine/carbon nanotube hybrid structures. *Nat. Commun.* **2017**, *8*, 1–8.
- (31) Hu, X. M.; Rønne, M. H.; Pedersen, S. U.; Skrydstrup, T.; Daasbjerg, K. Enhanced catalytic activity of cobalt porphyrin in CO_2 electroreduction upon immobilization on carbon materials. *Angew. Chem., Int. Ed.* **2017**, *56*, 6468–6472.
- (32) Abdinejad, M.; Dao, C.; Deng, B.; Dinic, F.; Voznyy, O.; Zhang, X.-A.; Kraatz, H.-B. Electrocatalytic reduction of CO_2 to CH_4 and CO in aqueous solution using pyridine-porphyrins immobilized onto carbon nanotubes. *ACS Sustainable Chem. Eng.* **2020**, *8*, 9549–9557.
- (33) Xu, F.; Zhang, L.; Ding, X.; Cong, M.; Jin, Y.; Chen, L.; Gao, Y. Selective electroreduction of dinitrogen to ammonia on a molecular iron phthalocyanine/O-MWCNT catalyst under ambient conditions. *Chem. Commun.* **2019**, *55*, 14111–14114.
- (34) Sinha, S.; Zhang, R.; Warren, J. J. Low overpotential CO_2 activation by a graphite-adsorbed cobalt porphyrin. *ACS Catal.* **2020**, 10, 12284–12291.
- (35) Vo, T. H.; Perera, U. G. E.; Shekhirev, M.; Mehdi Pour, M.; Kunkel, D. A.; Lu, H.; Gruverman, A.; Sutter, E.; Cotlet, M.; Nykypanchuk, D.; Zahl, P.; Enders, A.; Sinitskii, A.; Sutter, P. Nitrogen-doping induced self-assembly of graphene nanoribbon-based two-dimensional and three-dimensional metamaterials. *Nano Lett.* **2015**, *15*, 5770–5777.
- (36) Morgenroth, F.; Reuther, E.; Müllen, K. Polyphenylene dendrimers: from three-dimensional to two-dimensional structures. *Angew. Chem., Int. Ed.* **1997**, *36*, 631–634.
- (37) Vo, T. H.; Shekhirev, M.; Kunkel, D. A.; Morton, M. D.; Berglund, E.; Kong, L.; Wilson, P. M.; Dowben, P. A.; Enders, A.; Sinitskii, A. Large-scale solution synthesis of narrow graphene nanoribbons. *Nat. Commun.* **2014**, *5*, No. 3189.
- (38) Warren, J. J.; Tronic, T. A.; Mayer, J. M. Thermochemistry of proton-coupled electron transfer reagents and its implications. *Chem. Rev.* **2010**, *110*, 6961–7001.
- (39) Choi, J.; Wagner, P.; Gambhir, S.; Jalili, R.; MacFarlane, D. R.; Wallace, G. G.; Officer, D. L. Steric modification of a cobalt phthalocyanine/graphene catalyst to give enhanced and stable electrochemical CO2 reduction to CO. ACS Energy Lett. 2019, 4, 666–672.
- (40) Nam, D.-H.; De Luna, P.; Rosas-Hernández, A.; Thevenon, A.; Li, F.; Agapie, T.; Peters, J. C.; Shekhah, O.; Eddaoudi, M.; Sargent, E. H. Molecular enhancement of heterogeneous CO₂ reduction. *Nat. Mater.* **2020**, *19*, 266–276.
- (41) Sharifi, T.; Hu, G.; Jia, X.; Wagberg, T. Formation of active sites for oxygen reduction reactions by transformation of nitrogen functionalities in nitrogen-doped carbon nanotubes. *ACS Nano* **2012**, *6*, 8904–8912.

- (42) Brunetti, B.; De Giglio, E.; Cafagna, D.; Desimoni, E. XPS analysis of glassy carbon electrodes chemically modified with 8-hydroxyquinoline-5-sulphonic acid. *Surf. Interface Anal.* **2012**, *44*, 491–496.
- (43) Ramaswamy, N.; Tylus, U.; Jia, Q.; Mukerjee, S. Activity descriptor identification for oxygen reduction on nonprecious electrocatalysts: linking surface science to coordination chemistry. *J. Am. Chem. Soc.* **2013**, *135*, 15443–15449.
- (44) Lazar, P.; Mach, R.; Otyepka, M. Spectroscopic fingerprints of graphitic, pyrrolic, pyridinic, and chemisorbed nitrogen in N-doped graphene. *J. Phys. Chem. C* **2019**, *123*, 10695–10702.
- (45) Jackson, M. N.; Oh, S.; Kaminsky, C.; Chu, S. B.; Zhang, G.; Miller, J. T.; Surendranath, Y. Strong electronic coupling of molecular sites to graphitic electrodes via pyrazine conjugation. *J. Am. Chem. Soc.* **2018**, *140*, 1004–1010.
- (46) Fukushima, T.; Drisdell, W.; Yano, J.; Surendranath, Y. Graphite-Conjugated Pyrazines as Molecularly Tunable Heterogeneous Electrocatalysts. *J. Am. Chem. Soc.* **2015**, *137*, 10926–10929.